Journal of Solid State Chemistry 183 (2010) 10–19

Contents lists available at ScienceDirect

Journal of Solid State Chemistry

journal homepage: www.elsevier.com/locate/jssc

Neutron powder diffraction and first-principles computational studies of $CuLi_xMg_{2-x}$ ($x \cong 0.08$), $CuMg_2$, and Cu_2Mg

M.H. Braga [a,b,*], J.J.A. Ferreira [c], J. Siewenie [a], Th. Proffen [a], S.C. Vogel [a], L.L. Daemen [a]

[a] Manuel Lujan, Jr. Neutron Scattering Center, Los Alamos National Laboratory, Los Alamos, NM 87545, USA
[b] CEMUC and Physics Engineering Department, Engineering Faculty of the University of Porto, R. Dr. Roberto Frias, s/n, 4200-465 Porto, Portugal
[c] LNEG Laboratory, R. da Amieira-P.O. Box 1089, 4466-956 S. Mamede de Infesta, Portugal

ARTICLE INFO

Article history:
Received 18 June 2009
Received in revised form
9 September 2009
Accepted 13 September 2009
Available online 6 October 2009

Keywords:
Cu–Li–Mg
Neutron diffraction
First-principles calculations
X-ray diffraction
Rietveld refinement
Pair distribution function

ABSTRACT

A small addition of Li changes the orthorhombic structure of $CuMg_2$ to hexagonal $CuLi_xMg_{2-x}$ (x=0.08). Determining the Li content of the ternary phase and Li atomic positions was our main objective for this work. For this reason we performed neutron diffraction at several different temperatures below and above room temperature. The results obtained on two neutron powder diffractometers were compared with X-ray diffraction (XRD) data, and with first-principles calculations. The first-principles calculations are in good agreement with Rietveld-refined data from neutron diffraction, but do not show a marked preference for one of several possible Li sites. The pair distribution function (PDF) fitting is consistent with Li substituting only Mg1 (1/2, 0, z). Interstitial spaces in the structure of $CuMg_2$ and of $CuLi_xMg_{2-x}$ were also considered, but are unlikely to be occupied by Li. Neutron diffraction data for binary $CuMg_2$ and Cu_2Mg were also obtained.

Published by Elsevier Inc.

1. Introduction

Recently, we have solved by X-ray diffraction the structure of the only known ternary phase in the Cu–Li–Mg system [1]. Yet, some details about atoms' positions were left to be solved and so was the composition of the alloy.

The main reason for studying this system at the time was its relationship to the quaternary system Al–Cu–Li–Mg—a light alloy with possible applications in the transportation industry.

Another motivation for studying the $CuLi_xMg_{2-x}$ alloy is its possible use to store hydrogen [2–4]. Because the phase diagrams of Cu–Mg and Ni–Mg are similar, and because Cu and Ni have similar electron affinities, it was thought in the sixties that $CuMg_2$ would store hydrogen, too. However this is not the case [5]. $NiMg_2$ has a hexagonal structure ($P6_222$), but $CuMg_2$ has an orthorhombic structure (*Fddd*), and this structural difference is assumed to be the reason that $NiMg_2$ stores H_2 and forms a hydride, but $CuMg_2$ does not. $CuMg_2$ decomposes into Cu_2Mg and MgH_2 [5] upon hydrogen loading. As a result of this reaction and since $CuMg_2$ does not form a hydride, $CuMg_2$ was abandoned as a candidate material for hydrogen storage [5,6]. The hexagonal structure of $CuLi_xMg_{2-x}$, suggested the possibility of using this phase as a hydrogen storage material [2,3] because $CuLi_xMg_{2-x}$ has the same space group ($P6_222$) as $NiMg_2$ and $NiMg_2(H,D)_{0.3}$ (lattice parameters are almost identical: $a=b=5.250$ Å and $c=13.621$ Å (at 300 K) for $CuLi_xMg_{2-x}$ and $a=b=5.256$ Å and $c=13.435$ Å for $NiMg_2(H,D)_{0.3}$ [7]). Therefore, we hypothesized that $CuLi_xMg_{2-x}$ (x=0.08) would be a hydrogen storage material, just like $NiMg_2$—a hypothesis that has been confirmed by now [2–4].

In view of this it became important to determine the structure and composition of $CuLi_xMg_{2-x}$. In our previous work [1], two possibilities were raised for the structure and composition of the ternary disordered alloy, $CuLi_{0.34}Mg_2$ (in which Li occupies some of the Wyckoff 12*k* positions of a $P6_222$ hexagonal structure) and $CuLi_{0.106}Mg_{1.894}$ (in which Li occupies some of the Mg Wyckoff 6*f* positions of a $P6_222$ hexagonal structure). It was not possible to distinguish between these possibilities using X-ray diffraction, owing to the weak scattering of X-rays by Li. While Li is not a strong coherent neutron scatterer, measurements with neutrons coupled to first-principles calculations offer a complementary approach to the determination of the most stable structure and to the most stable composition.

The change of the $CuMg_2$ orthorhombic (*Fddd*) structure to a hexagonal structure ($P6_2222$) upon addition of a small amount of Li has been firmly established [1]. Isostructural phases to $CuLi_xMg_{2-x}$ are the hexagonal phase $NiMg_2$ and $NiMg_2H_{0.24-0.30}$ [7]. For the NiMg-hydrides, several hydrogen positions were

* Corresponding author at: CEMUC and Physics Engineering Department, Engineering Faculty of the University of Porto, R. Dr. Roberto Frias, s/n, 4200-465 Porto, Portugal. Fax: +351 225081447.
E-mail address: mbraga@fe.up.pt (M.H. Braga).

0022-4596/$ - see front matter Published by Elsevier Inc.
doi:10.1016/j.jssc.2009.09.010

reported: In $NiMg_2H_{0.29}$ the hydrogen atoms occupy Wyckoff 6*f* positions [7] and could occupy the interstitial Wyckoff 6*h* position [7]. Other possibilities would be that the H atoms would just occupy interstitial Wyckoff 12*k* position (in $NiMg_2H_{0.26}$) or the Wyckoff 12*k* and 6*j* positions in $NiMg_2H_{0.24}$ [7]. This suggests a number of possible sites for Li in $CuLi_xMg_{2-x}$.

Interestingly Hlukhyy et al. [8] have reported a result closely related to our observations in the Sn-doped Ni–Mg system. These authors show that the synthesis of alloys in the Ni–Mg system is affected by the presence of small amounts of Sn (forming $NiMg_{2-x}Sn_x$ with x=0.22 and 0.40). The replacement of Mg by Sn produces changes in the structure of $NiMg_2$, this time making the alloy change from the $NiMg_2$ type (hexagonal) to the $CuMg_2$ type (orthorhombic). While the structure of $NiMg_{1.85}Sn_{0.15}$ is still of $NiMg_2$ type, the structure of $NiMg_{1.78}Sn_{0.22}$ and $NiMg_{1.60}Sn_{0.40}$ is already of the $CuMg_2$ type. These results represent obviously the converse of our own observations in the $CuMg_2$ structure, and reaffirm our results with respect to $CuLi_xMg_{2-x}$. Again, this suggests possibilities for Li atomic sites.

Table 1
Rietveld refinement's results at 60, 150 and 300 K obtained from NPDF data.

T=60 K (NPDF) wR_p=2.01%; R_p=1.38% Wt. Frac. ($CuLi_{0.069}Mg_{1.931}$)=0.356 (4); Wt. Frac. ($CuMg_2$)=0.426 (4); Wt. Frac. (Cu_2Mg)=0.218 (3)		
$CuLi_{0.069}Mg_{1.917}$ Hexagonal–$P6_222$ (180) a=b=5.2476 (3) Å; c=13.6193 (9) Å; ρ=3.404 g/cm^3	$CuMg_2$ Orthorhombic–Fddd (70) a=5.2622 (3) Å; b=9.0207 (6) Å; c=18.310 (1) Å; ρ=3.428 g/cm^3	Cu_2Mg Cubic–Fd-3m (227) a=b=c=7.0607 (4) Å; ρ=5.714 g/cm^3
Cu1: x=0; y=0; $z=\frac{1}{2}$; occ.=1; $U_{iso}\times100$=0.49 (2) Å^2 Cu2: $x=\frac{1}{2}$; y=0; $z=\frac{1}{2}$; occ.=1; $U_{iso}\times100$=0.42 (3) Å^2 Mg1: $x=\frac{1}{2}$; y=0; z=0.1124 (1); occ.=0.931 (7); $U_{iso}\times100$=0.50 (3) Å^2 Mg2: x=0.1663 (4); y=0.3326 (9); z=0; occ.=1; $U_{iso}\times100$=0.85 (4) Å^2 Li1: $x=\frac{1}{2}$; y=0; z=0.1124 (1); occ.=0.069 (7); $U_{iso}\times100$=0.50 (3) Å^2	Cu1: $x=\frac{1}{8}$; $y=\frac{1}{8}$; z=0.49851 (5); occ.=1; $U_{iso}\times100$=0.29 (2) Å^2 Mg1: $x=\frac{1}{8}$; $y=\frac{1}{8}$; z=0.04164 (8); occ.=1; $U_{iso}\times100$=0.65 (3) Å^2 Mg2: $x=\frac{1}{8}$; y=0.4591 (2); $z=\frac{1}{8}$; occ.=1; $U_{iso}\times100$=0.55 (3) Å^2	Cu1: x=0; y=0; z=0; occ.=1; $U_{iso}\times100$=0.55 (1) Å^2 Mg1: $x=\frac{3}{8}$; $y=\frac{3}{8}$; $z=\frac{3}{8}$; occ.=1; $U_{iso}\times100$=0.67 (2) Å^2
T=150 K (NPDF) wR_p=2.01%; R_p=1.37% Wt. Frac. ($CuLi_{0.083}Mg_{1.931}$)=0.357 (4); Wt. Frac. ($CuMg_2$)=0.424 (4); Wt. Frac. (Cu_2Mg)=0.219 (3)		
$CuLi_{0.083}Mg_{1.917}$ Hexagonal–$P6_222$ (180) a=b=5.2483 (4) Å c=13.620 (1) Å; ρ=3.395 g/cm^3	$CuMg_2$ Orthorhombic–Fddd (70) a=5.2625 (4) Å; b=9.0233 (7) Å c=18.309 (1) Å; ρ=3.427 g/cm^3	Cu_2Mg Cubic–Fd-3m (227) a=b=c=7.0608 (4) Å ρ=5.713 g/cm^3
Cu1: x=0; y=0; $z=\frac{1}{2}$; occ.=1; $U_{iso}\times100$=0.77 (3) Å^2 Cu2: $x=\frac{1}{2}$; y=0; $z=\frac{1}{2}$; occ.=1; $U_{iso}\times100$=0.65 (4) Å^2 Mg1: $x=\frac{1}{2}$; y=0; z=0.1123 (2); occ.=0.917 (7); $U_{iso}\times100$=0.66 (5) Å^2 Mg2: x=0.1666 (5); y=0.333 (1); z=0; occ.=1; $U_{iso}\times100$=1.11 (5) Å^2 Li1: $x=\frac{1}{2}$; y=0; z=0.1123 (2); occ.=0.083 (7); $U_{iso}\times100$=0.66 (5) Å^2	Cu1: $x=\frac{1}{8}$; $y=\frac{1}{8}$; z=0.49860 (5); occ.=1; $U_{iso}\times100$=0.52 (2) Å^2 Mg1: $x=\frac{1}{8}$; $y=\frac{1}{8}$; z=0.04152 (8); occ.=1; $U_{iso}\times100$=0.86 (3) Å^2 Mg2: $x=\frac{1}{8}$; y=0.4594 (2); $z=\frac{1}{8}$; occ.=1; $U_{iso}\times100$=0.77 (3) Å^2	Cu1: x=0; y=0; z=0; occ.=1; $U_{iso}\times100$=0.81 (2) Å^2 Mg1: $x=\frac{3}{8}$; $y=\frac{3}{8}$; $z=\frac{3}{8}$; occ.=1; $U_{iso}\times100$=0.92 (3) Å^2
T=300 K (NPDF) wR_p=1.93%; R_p=1.29% Wt. Frac. ($CuLi_{0.083}Mg_{1.931}$)=0.351 (5); Wt. Frac. ($CuMg_2$)=0.427 (5); Wt. Frac. (Cu_2Mg)=0.222 (3)		
$CuLi_{0.083}Mg_{1.931}$ Hexagonal–$P6_222$ (180) a=b=5.2495 (5) Å; c=13.621 (1) Å; ρ=3.401 g/cm^3	$CuMg_2$ Orthorhombic–Fddd (70) a=5.2625 (5) Å; b=9.0278 (8) Å c=18.307 (2) Å; ρ=3.426 g/cm^3	Cu_2Mg Cubic–Fd-3m (227) a=b=c=7.0598 (6) Å ρ=5.716 g/cm^3
Cu1: x=0; y=0; $z=\frac{1}{2}$; occ.=1; $U_{iso}\times100$=1.26 (4) Å^2 Cu2: $x=\frac{1}{2}$; y=0; $z=\frac{1}{2}$; occ.=1; $U_{iso}\times100$=1.09 (5) Å^2 Mg1: $x=\frac{1}{2}$; y=0; z=0.1123 (2); occ.=0.917 (8); $U_{iso}\times100$=1.15 (7) Å^2 Mg2: x=0.1669 (6); y=0.334 (1); z=0; occ.=1; $U_{iso}\times100$=1.66 (6) Å^2 Li1: $x=\frac{1}{2}$; y=0; z=0.1123 (2); occ.=0.083 (8); $U_{iso}\times100$=1.15 (7) Å^2	Cu1: $x=\frac{1}{8}$; $y=\frac{1}{8}$; z=0.49860 (6); occ.=1; $U_{iso}\times100$=0.98 (2) Å^2 Mg1: $x=\frac{1}{8}$; $y=\frac{1}{8}$; z=0.0415 (1); occ.=1; $U_{iso}\times100$=1.41 (4) Å^2 Mg2: $x=\frac{1}{8}$; y=0.4598 (3); $z=\frac{1}{8}$; occ.=1; $U_{iso}\times100$=1.35 (4) Å^2	Cu1: x=0; y=0; z=0; occ.=1; $U_{iso}\times100$=1.27 (2) Å^2 Mg1: $x=\frac{3}{8}$; $y=\frac{3}{8}$; $z=\frac{3}{8}$; occ.=1; $U_{iso}\times100$=1.41 (3) Å^2

Note: $R_p=\sum|I_o-I_c|/\sum I_o$ and $wR_p=[\sum w(I_o-I_c)^2/\sum wI_o^2]^{1/2}$, in which I_o is the observed intensity, I_c is the calculated one. The weights, w, are derived from an error propagation scheme.

2. Material and methods

2.1. Synthesis and characterization

The Cu–Li–Mg samples were prepared with a target composition of $CuLi_{0.10}Mg_{1.90}$ and $CuLi_{0.34}Mg_2$. They were prepared by mixing stoichiometric amounts of Cu (electrolytic, 99.99% purity, 325 mesh), Mg (99.8% purity, 200 mesh, Alfa Aesar), and small (less than 3 mm wide) pieces of Li (99% purity, Alfa Aesar). Because of the large vapor pressure of Mg, even below its melting point, the reagents were sealed in a stainless steel crucible in a dry box with He atmosphere. This had the added advantage of minimizing possible reagent loss. The samples were heated in a tube furnace with a stirring device to ensure proper mixing of the heterogeneous starting mixture and complete dispersion of Li in the sample. Different reaction temperatures and times were used. Regardless of reaction conditions, the samples, as investigated by XRD, invariably contained Cu_2Mg, $CuMg_2$, or both (but no pure metals). Nonetheless, we obtained final products containing approximately up to 81.0 wt% (75.6 at%) of $CuLi_xMg_{2-x}$. Since the structures of Cu_2Mg and $CuMg_2$ are known (and they are confirmed in this paper), this complication translated merely in the refinement of two additional phases in the neutron powder diffraction pattern.

We studied two samples with very different compositions, both of them containing $CuLi_xMg_{2-x}$, $CuMg_2$ and Cu_2Mg: 70.4 at% $CuLi_xMg_{2-x}$, 21.0 at% $CuMg_2$, 8.6 at% Cu_2Mg in the first sample and 38.0 at% $CuLi_xMg_{2-x}$, 44.8 at% $CuMg_2$, 17.2 at% Cu_2Mg. By means of XRD, we have studied previously a sample with: 75.6 at% of $CuLi_xMg_{2-x}$ and 24.4 at% of Cu_2Mg [9].

Samples were first characterized by means of XRD using a Rigaku Ultima III powder diffractometer, and their composition was roughly determined by means of the Match software [10], which uses the "reference intensity ratio method" (RiR-method) [11] to obtain phase fractions. Patterns were collected with Cu$K\alpha$ typically from 2θ=15 to 70° with steps of 0.02° and a counting time of 10 s per bin.

2.2. Powder X-ray diffraction measurements

At room temperature, some powder samples were measured on a Philips X'Pert Pro MPD using Cu$K\alpha_1$ radiation (λ=0.15406 nm) monochromated by a symmetric Ge (111) crystal [1]. When those samples were studied at high temperatures, instead of the primary monochromated monochromatic radiation, Cu$K\alpha_1$ and Cu$K\alpha_2$ (λ=0.15443 nm) were used, because the intensity of the incident/diffracted beam was already attenuated by the protective graphite foil of the heating chamber. Intensity can become crucial when a sample is being heated because the counting time cannot be very high owing to the sample's reactivity. The heating chamber was an Anton Parr that operates from room temperature to 1473 K in vacuum ($\lesssim 10^{-5}$ mbar) or in argon atmosphere. Patterns were collected from 5 to 120° (2θ)

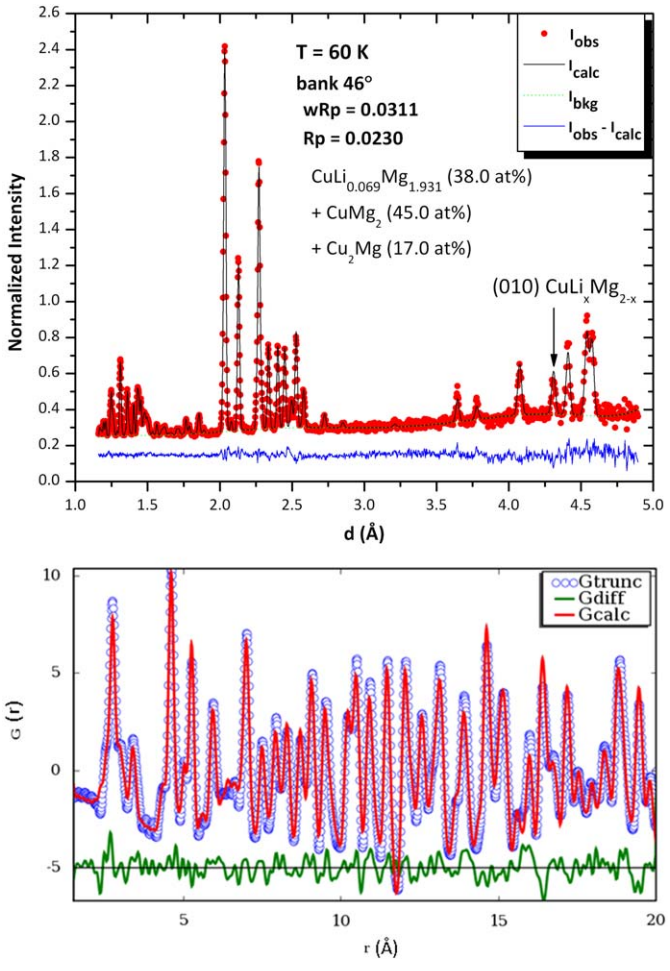

Fig. 1. NPDF after Rietveld refinement diffraction pattern at 60 K for 46° bank (the results at the graph are only due to the 46° bank). PDF experimental and fitted.

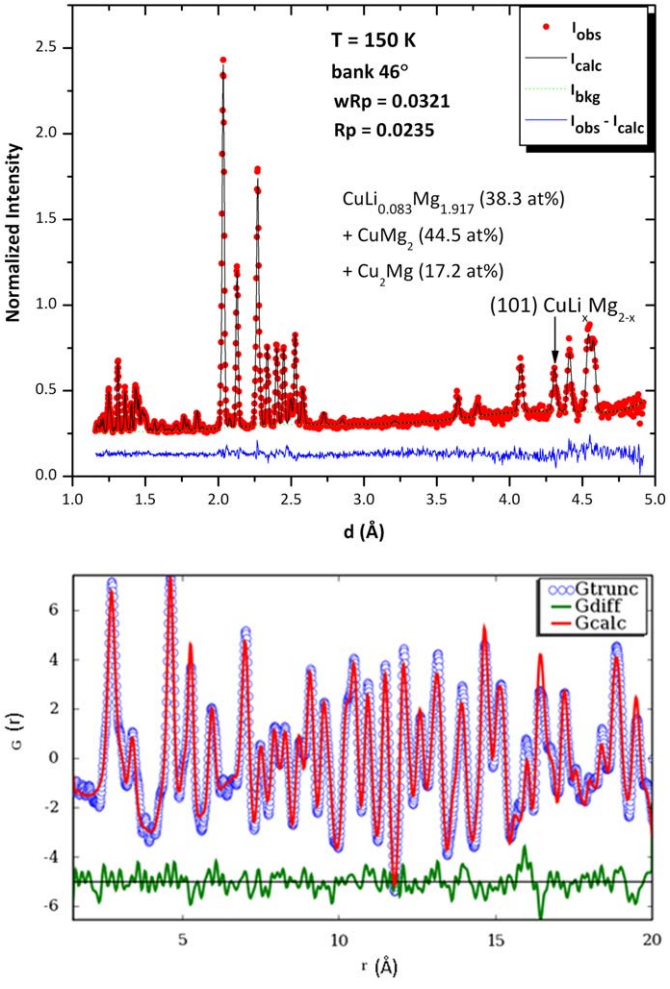

Fig. 2. NPDF after Rietveld refinement diffraction pattern at 150 K for 46° bank (the results at the graph are only due to the 46° bank). PDF experimental and fitted.

with steps of 0.01° and a counting time of 10 s at 303, 473, 523, 573 and 623 K [9]. Results from differential scanning calorimeter (DSC) have shown that $CuLi_xMg_{2-x}$ decomposes at approximately 702 K [9].

2.3. Neutron powder diffraction measurements (below room temperature)

Time-of-flight (TOF) neutron diffraction data were collected on the NPDF neutron diffractometer at the Manuel Lujan Neutron Scattering Center at Los Alamos National Laboratory. This instrument is a high-resolution powder diffractometer located 32 m from the neutron spallation target. The data were collected at 60 K (for 7.7 h), 150 K (for 6.4 h) and 300 K (for 6.2 h), at an average proton beam current of 100 μA, using the 46, 90, 119 and 148° banks, which cover a *d*-spacing range from 0.12 to 7.2 Å. A sample powder with 38.0 at% of $CuLi_xMg_{2-x}$, 44.8 at% of $CuMg_2$ and 17.2 at% of Cu_2Mg was manually grinded to a diameter of less than 37 μm and placed in a vanadium sample holder in a glove box under He. The vanadium sample holder contribution, at each *T*, was subsequently removed from the diffraction pattern. The structure was refined using the general structure analysis system (GSAS), a Rietveld profile analysis program developed by Larson and von Dreele [12]. Background coefficients, scale factors, phase fractions, profile function coefficients (sigma-1), sample absorption, atomic positions, lattice parameters, temperature factors, and occupancies (in the case of the phase $CuLi_xMg_{2-x}$ and for Mg and Li) were refined for the three phases (whenever applicable) making a total of 81 variables.

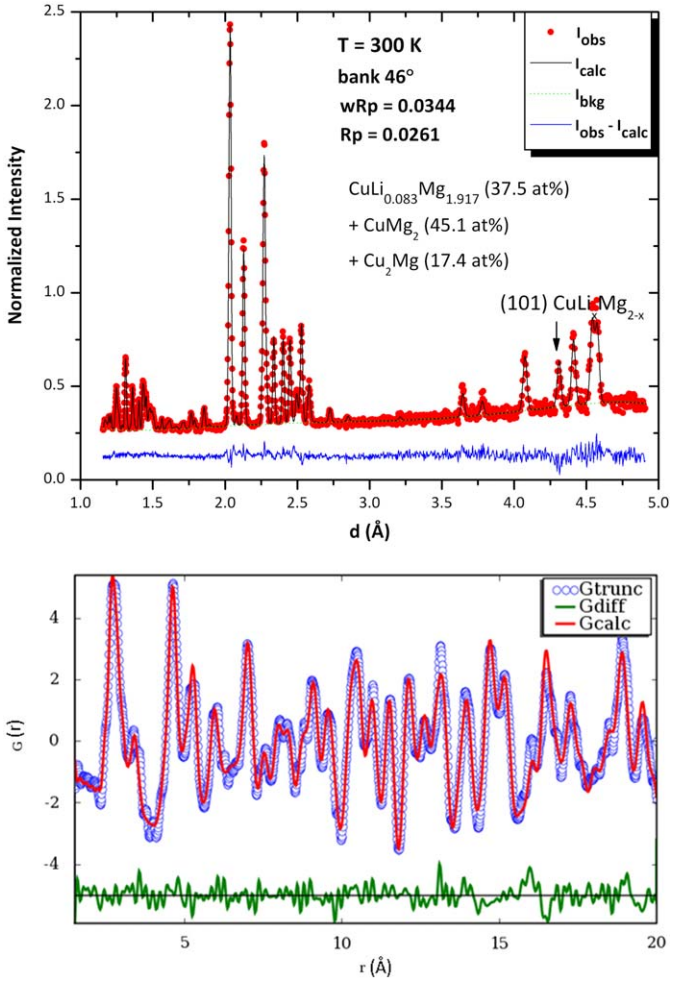

Fig. 3. NPDF after Rietveld refinement diffraction pattern at 300 K for 46° bank (the results at the graph are only due to the 46° bank). PDF experimental and fitted.

For NPDF data, pair distribution function (PDF), $G(r)$, was obtained via the Fourier Transform of the total diffraction pattern as indicated below,

$$G(r) = 4\pi r[\rho(r) - \rho_0] = \frac{2}{r}\int_0^{\infty} Q[S(Q) - 1]\sin(Qr)\,dQ \quad (1)$$

where $\rho(r)$ is the microscopic pair density, ρ_0 is the average atomic number density, and r the radial distance. Q is the momentum transfer ($Q = 4\pi\sin(\theta)/\lambda$). $S(Q)$ is the normalized structure function determined from the experimental diffraction intensity [13]. PDF yields the probability of finding pairs of atoms separated by a distance *r*. PDF fittings were performed using the software PDFgui [14].

2.4. Neutron powder diffraction measurements (above room temperature)

Time-of-flight (TOF) neutron diffraction data were also collected on the neutron powder diffractometer (HIPPO) at the Manuel Lujan Neutron Scattering Center at Los Alamos National Laboratory. This instrument achieves very high neutron count rates by virtue of a short (9 m) flight path and large detector solid angle. The data were collected at approx. 313 K (for 1.6 h), 373 K (for 6.3 h), 453 K (for 2 h) and 523 K (for 0.90 h), at an average proton beam current of 100 μA, using the 90, and 144.45° banks, which cover a *d*-spacing range from 0.12 to 4.80 Å.

A sample powder with 70.4 at% of $CuLi_xMg_{2-x}$, 21.0 at% of $CuMg_2$ and 8.6 at% of Cu_2Mg was enclosed in an aluminum sample holder to which a resistive heater and a thermocouple was attached. A standard laboratory temperature controller maintained the desired temperature during the measurement. A capillary tube attached to the sample holder allowed for pressure measurements and gas loading during the experiments.

The aluminum sample holder contributes to the diffraction pattern. An aluminum phase was refined in all our data sets. The measured sample (including Al) had: 42.1 wt% (14.6 at%) of $CuLi_xMg_{2-x}$+$CuMg_2$+Cu_2Mg and 57.9 wt% (86.4 at%) of Al. The structure was refined using GSAS. Background coefficients, scale factors, phase fractions, profile function coefficients (sigma-1),

Table 2
PDF fittings' results at 60, 150 and 300 K obtained from NPDF data.

T=60 K (NPDF) R_{wp}=18.6%		
$CuLi_xMg_{2-x}$ (x=0.03 ± 0.04)	$CuMg_2$	Cu_2Mg
Hexagonal–$P6_222$ (180)	Orthorhombic–Fddd (70)	Cubic–Fd-3m (227)
a=b=5.250 (2) Å; c=13.666 (7) Å;	a=5.240 (5) Å; b=9.003 (8) Å; c=18.25 (2) Å	a=b=c=7.058 (2) Å;
T=150 K (NPDF) R_{wp}=17.6%		
$CuLi_xMg_{2-x}$ (x=0.10 ± 0.04)	$CuMg_2$	Cu_2Mg
Hexagonal–$P6_222$ (180)	Orthorhombic–Fddd (70)	Cubic–Fd-3m (227)
a=b=5.258 (3) Å; c=13.67 (1) Å	a=5.248 (8) Å; b=9.01 (1) Å; c=18.25 (2) Å	a=b=c=7.066 (2) Å
T=300 K (NPDF) R_{wp}=17.6%		
$CuLi_xMg_{2-x}$ (x=0.08 ± 0.06)	$CuMg_2$	Cu_2Mg
Hexagonal–$P6_222$ (180)	Orthorhombic–Fddd (70)	Cubic–Fd-3m (227)
a=b=5.273 (4) Å; c=13.70 (2) Å	a=5.30 (2) Å; b=9.00 (2) Å c=17.92 (5) Å	a=b=c= 7.082 (4)

sample absorption, atomic positions, lattice parameters, temperature factors, and occupancies (in the case of the phase $CuLi_xMg_{2-x}$ and for Mg and Li) were refined for the four phases (whenever applicable) making a total of 63 variables.

3. First principles data

In a solid, where there are upward of 10^{24} interacting electrons and nuclei per cubic centimeter, the resolution of the many body Schrödinger equation for the electronic wavefunctions and energy eigenvalues is a big challenge. However, based on the periodicity of the structure of pure elements and perfectly ordered compounds, Bloch's theorem shows that it is only necessary to solve the many body Schrödinger equation within one unit cell; in the case of disordered compounds that is not the case and it is necessary to solve it within a supercell. The basic information that one wishes to obtain from quantum mechanical calculations in solids is the total electronic energy for various arrangements of atoms on various lattices.

One of the most sophisticated solutions to the quantum mechanical problem in solids lies within the framework of the density functional theory (DFT) [15] using the local density approximation (LDA) [16] or the Generalized Gradient Approximation (GGA) [17]. The basic notion of these theories is to replace the true interacting many-body-system with a system of one electron in an effective potential due to all of the other electrons and nuclei. From a fundamental point of view, the one-electron functions are a unique tool for calculating the total energy and the electronic density of states; these functions have no particular physical meaning. But this simplification of the problem needs a self-consistent calculation and it is one of the major technical problems in the *ab initio* approach [18].

Density functional theory calculations with projector augmented wave (PAW) pseudopotentials [19], as implemented in the Vienna *Ab Initio* Simulation Package (VASP) code [20], implemented in MedeA [21], were performed. A plane wave cutoff of 355.18 eV, and *k*-spacings of $0.230 \times 0.230 \times 0.230\,\text{Å}^{-1}$ were used. Calculations were done in real space and were performed with *P*1 space group supercells containing 144 atoms (48 atoms of Cu, 96-*n* of Mg, and *n*=0 to 12 of Li). The supercells contained as many atoms as possible to allow better approximations with the real Li concentrations (but such that the time spent on calculations were not completely impractical). Since $CuLi_xMg_{2-x}$ is a disordered structure, it had to be obtained by randomly substituting Mg by Li in several Wyckoff 6*f* positions (1/2, 0, *z*) or Wyckoff 6*i* positions (*x*, 2*x*, 0) or in both positions within the supercells. The generalized gradient approximation (GGA), and the Perdew–Burke–Ernzerhof (PBE) functional [22] were used, and no magnetic moments were included in the model.

The total energy was minimized with respect to the volume (volume relaxation), the shape of the unit cell (cell external relaxation), and the position of the atoms within the cell (cell internal relaxation).

The *ab initio* calculations furnish the total energy (or the cohesive energy) at $T=0$ K, E^{Φ}. The energy of formation is easily

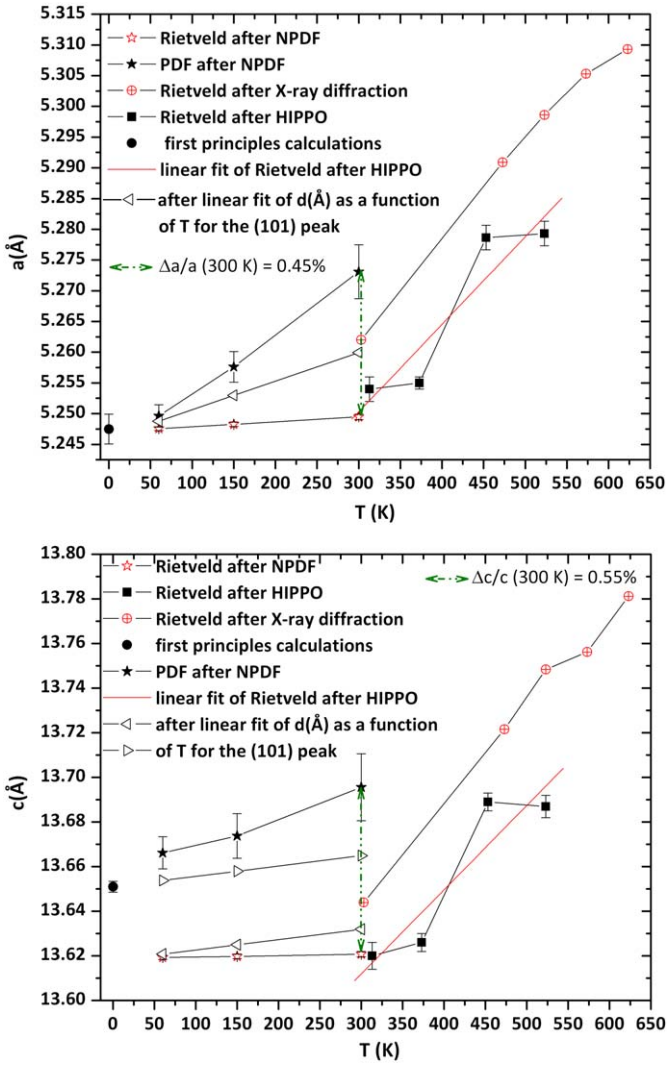

Fig. 4. Lattice parameters of the phase $CuLi_xMg_{2-x}$ as a function of the absolute temperature. It can be observed a linear dependence from the lattice parameters towards the temperature between 60 and 300 K as well as a small difference between lattice parameters obtained by first principles and obtained after refinement of the experimental data. Notice that the slope of the fitting line between 300 and 523 K is very similar to that obtained by X-ray diffraction [9]. It can also be observed that results obtained by PDF fitting differ 0.45% in the case of *a* and 0.55% in the case of *c*, at 300 K. Lattice parameters calculated using the slope obtained after plotting the interatomic distance *d*, as a function of temperature for the (101) peak were also plotted (note that the only peaks that were not overlapped with peaks from another phase, depend on *a* and *c*). As the phase is not isotropic, the use of this value is not completely correct. Nonetheless, it allows us to be more confident about the non-interference of $CuLi_xMg_{2-x}$ and $CuMg_2$ during calculations, since these two phases have several overlapping peaks.

One of the most sophisticated solutions to the quantum mechanical problem in solids lies within the framework of the density functional theory (DFT) [15] using the local density approximation (LDA) [16] or the Generalized Gradient Approximation (GGA) [17]. The basic notion of these theories is to replace the true interacting many-body-system with a system of one electron in an effective potential due to all of the other electrons and nuclei. From a fundamental point of view, the one-electron functions are a unique tool for calculating the total energy and the electronic density of states; these functions have no particular physical meaning. But this simplification of the problem needs a self-consistent calculation and it is one of the major technical problems in the *ab initio* approach [18].

Density functional theory calculations with projector augmented wave (PAW) pseudopotentials [19], as implemented in the Vienna *Ab Initio* Simulation Package (VASP) code [20], implemented in MedeA [21], were performed. A plane wave cutoff of 355.18 eV, and *k*-spacings of $0.230 \times 0.230 \times 0.230\,\text{Å}^{-1}$ were used. Calculations were done in real space and were performed with *P*1 space group supercells containing 144 atoms (48 atoms of Cu, 96-*n* of Mg, and *n*=0 to 12 of Li). The supercells contained as many atoms as possible to allow better approximations with the real Li concentrations (but such that the time spent on calculations were not completely impractical). Since $CuLi_xMg_{2-x}$ is a disordered structure, it had to be obtained by randomly substituting Mg by Li in several Wyckoff 6*f* positions (1/2, 0, *z*) or Wyckoff 6*i* positions (*x*, 2*x*, 0) or in both positions within the supercells. The generalized gradient approximation (GGA), and the Perdew–Burke–Ernzerhof (PBE) functional [22] were used, and no magnetic moments were included in the model.

The total energy was minimized with respect to the volume (volume relaxation), the shape of the unit cell (cell external relaxation), and the position of the atoms within the cell (cell internal relaxation).

The *ab initio* calculations furnish the total energy (or the cohesive energy) at $T=0$ K, E^{Φ}. The energy of formation is easily

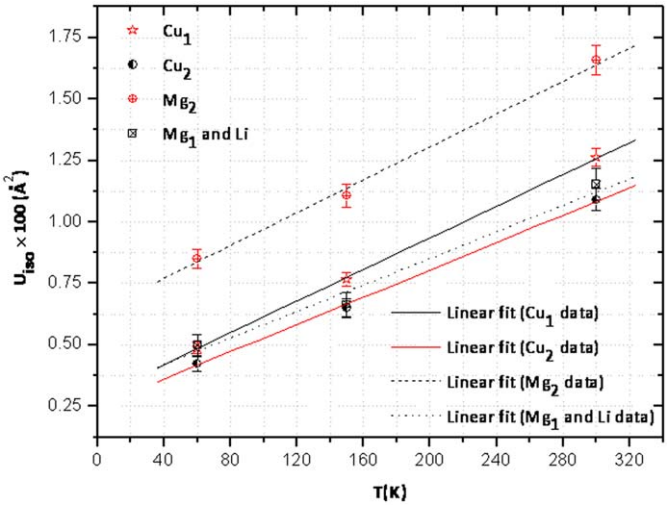

Fig. 5. Isotropic temperature factors for all the atoms of the phase $CuLi_xMg_{2-x}$ as a function of the absolute temperature. It can be seen that between 60 and 300 K all temperature factors behave linearly and increase similarly with temperature. U_{iso} is related with the Debye–Waller factor, B_{iso}, by: $B_{iso}=8\pi^2U_{iso}$.

calculated by the relation

$$\Delta_f E = E^{\Phi} - \sum x_i E_i^O \quad (2)$$

where E_i^O is the total energy (or cohesive energy) of i in its stable state at T=0 K. In the following we will assume that the enthalpy of formation is equal to the energy of formation.

In addition to the total energies, *ab initio* calculations allowed us to obtain the values of the lattice parameters at 0 K. We performed most of the calculations for $CuLi_xMg_{2-x}$ at least twice (from 1 to 5 atoms of Li calculations were performed three or more times) with different random Li positions.

We also calculated the X-ray diffraction pattern from the *ab initio* results. The code is implemented in MedeA and is based on the LAZY-PULVERIX computer program [23] that calculates the position of the diffraction lines from Bragg's law and their d-spacings. The diffraction intensity I_{hkl} is calculated as,

$$I_{hkl} = MLPF_{hkl}^2 \quad (3)$$

where M is the multiplicity factor of a powder line, L is the Lorentz factor and P is the polarization factor. The structure factor F_{hkl} is defined by,

$$F_{hkl} = \sum_{i}^{unit\text{-}cell} f_j O_j \exp[2\pi i(hx_j + kx_j + lz_j)] \exp\left(-B_j \frac{\sin^2\theta}{\lambda^2}\right) \quad (4)$$

where f_j is the atomic scattering factor of atom j, O_j is the occupation factor at site x_j, y_j, z_j, for atom j and B_j the Debye–Waller factor in Å^2 for atom j.

Table 3
Rietveld refinement's results at 313, 373, 453 and 523 K obtained from NPDF data.

~313 K (HIPPO) wR_p=3.79%; R_p=2.89% Wt. Frac. ($CuLi_{0.09}Mg_{1.91}$)=0.280 (8); Wt. Frac. ($CuMg_2$)=0.090 (3); Wt. Frac. (Cu_2Mg)=0.041 (1); Wt. Frac. (Al)=0.589 (7); $CuLi_{0.09}Mg_{1.91}$: hexagonal–$P6_222$ (180) a=b=5.254 (2) Å; c=13.620 (6) Å; ρ=3.384 g/cm^3	$CuMg_2$: orthorhombic–Fddd (70) a=5.264 (4) Å; b=9.026 (5) Å ; c=18.33 (1) Å; ρ=3.422 g/cm^3
Cu1: x=0; y=0; $z=\frac{1}{2}$; occ.=1; $U_{iso}\times100$=1.3 (1) Å^2 Cu2: $x=\frac{1}{2}$; y=0; $z=\frac{1}{2}$; occ.=1; $U_{iso}\times100$=1.4 (1) Å^2 Mg1: $x=\frac{1}{2}$; y=0; z=0.1092 (4); occ.=0.91 (2); $U_{iso}\times100$=1.4 (2) Å^2 Mg2: x=0.164 (1); y=0.328 (2); z=0; occ.=1; $U_{iso}\times100$=2.1 (2) Å^2 Li1: $x=\frac{1}{2}$; y=0; z=0.1092 (4); occ.=0.09 (2); $U_{iso}\times100$=1.4 (2) Å^2	
~373 K (HIPPO) wR_p=3.52%; R_p=2.36% Wt. Frac. ($CuLi_{0.08}Mg_{1.92}$)=0.297 (5); Wt. Frac. ($CuMg_2$)=0.083 (3); Wt. Frac. (Cu_2Mg)=0.051 (2); Wt. Frac. (Al)=0.569 (5); $CuLi_{0.08}Mg_{1.92}$: hexagonal–$P6_222$ (180) a=b=5.255 (1) Å; c=13.626 (4) Å ρ=3.386 g/cm^3	$CuMg_2$: orthorhombic–Fddd (70) a=5.262 (2) Å; b=9.033 (3) Å c=18.327 (6) Å; ρ=3.420 g/cm^3
Cu1: x=0; y=0; $z=\frac{1}{2}$; occ.=1; $U_{iso}\times100$=1.64 (9) Å^2 Cu2: $x=\frac{1}{2}$; y=0; $z=\frac{1}{2}$; occ.=1; $U_{iso}\times100$=1.04 (1) Å^2 Mg1: $x=\frac{1}{2}$; y=0; z=0.1111 (3); occ.=0.919 (8); $U_{iso}\times100$=1.5 (1) Å^2 Mg2: x=0.1719 (7); y=0.344 (1); z=0; occ.=1; $U_{iso}\times100$=2.0 (1) Å^2 Li1: $x=\frac{1}{2}$; y=0; z=0.1111 (3); occ.=0.081 (8); $U_{iso}\times100$=1.5 (1) Å^2	Cu1: $x=\frac{1}{8}$; $y=\frac{1}{8}$; z=0.4976 (3); occ.=1; $U_{iso}\times100$=1.3 (2) Å^2 Mg1: $x=\frac{1}{8}$; $y=\frac{1}{8}$; z=0.0416 (6); occ.=1; $U_{iso}\times100$=1.1 (3) Å^2 Mg2: $x=\frac{1}{8}$; y=0.4708 (1); $z=\frac{1}{8}$; occ.=1; $U_{iso}\times100$=1.37 (3) Å^2
~453 K (HIPPO) wR_p=3.38%; R_p=2.28% Wt. Frac. ($CuLi_{0.09}Mg_{1.91}$)=0.300 (6); Wt. Frac. ($CuMg_2$)=0.088 (3); Wt. Frac. (Cu_2Mg)=0.053 (2); Wt. Frac. (Al)=0.559 (6); $CuLi_{0.09}Mg_{1.91}$: hexagonal–$P6_222$ (180) a=b=5.279 (2) Å; c=13.689 (4) Å ρ=3.337 g/cm^3	$CuMg_2$: orthorhombic–Fddd (70) a=5.286 (2) Å; b=9.072 (3) Å c=18.406 (7) Å; ρ=3.376 g/cm^3
Cu1: x=0; y=0; $z=\frac{1}{2}$; occ.=1; $U_{iso}\times100$=1.9 (1) Å^2 Cu2: $x=\frac{1}{2}$; y=0; $z=\frac{1}{2}$; occ.=1; $U_{iso}\times100$=1.51 (9) Å^2 Mg1: $x=\frac{1}{2}$; y=0; z=0.1106 (3); occ.=0.91 (1); $U_{iso}\times100$=2.0 (1) Å^2 Mg2: x=0.1712 (8); y=0.342 (2); z=0; occ.=1; $U_{iso}\times100$=2.4 (1) Å^2 Li1: $x=\frac{1}{2}$; y=0; z=0.1106 (3); occ.=0.09 (1); $U_{iso}\times100$=2.0 (1) Å^2	Cu1: $x=\frac{1}{8}$; $y=\frac{1}{8}$; z=0.4984 (4); occ.=1; $U_{iso}\times100$=1.6 (3) Å^2 Mg1: $x=\frac{1}{8}$; $y=\frac{1}{8}$; z=0.0411 (6); occ.=1; $U_{iso}\times100$=1.3 (3) Å^2 Mg2: $x=\frac{1}{8}$; y=0.4741 (2); $z=\frac{1}{8}$; occ.=1; $U_{iso}\times100$=2.63 (3) Å^2
~523 K (HIPPO) wR_p=2.71%; R_p=1.91% Wt. Frac. ($CuLi_{0.09}Mg_{1.91}$)=0.282 (6); Wt. Frac. ($CuMg_2$)=0.089 (4); Wt. Frac. (Cu_2Mg)=0.050 (2); Wt. Frac. (Al)=0.579 (6); $CuLi_{0.09}Mg_{1.91}$: hexagonal–$P6_222$ (180) a=b=5.279 (2) Å; c=13.687 (5) Å ρ=3.334 g/cm^3	$CuMg_2$: orthorhombic–Fddd (70) a=5.285 (2) Å; b=9.076 (4) Å c=18.406 (8) Å; ρ=3.374 g/cm^3
Cu1: x=0; y=0; $z=\frac{1}{2}$; occ.=1; $U_{iso}\times100$=1.9 (1) Å^2 Cu2: $x=\frac{1}{2}$; y=0; $z=\frac{1}{2}$; occ.=1; $U_{iso}\times100$=1.55 (1) Å^2 Mg1: $x=\frac{1}{2}$; y=0; z=0.1093 (4); occ.=0.91 (1); $U_{iso}\times100$=2.0 (2) Å^2 Mg2: x=0.1692 (9); y=0.338 (2); z=0; occ.=1; $U_{iso}\times100$=2.3 (2) Å^2 Li1: $x=\frac{1}{2}$; y=0; z=0.1093 (4); occ.=0.09 (1); $U_{iso}\times100$=2.0 (2) Å^2	Cu1: $x=\frac{1}{8}$; $y=\frac{1}{8}$; z=0.4978 (4); occ.=1; $U_{iso}\times100$=1.5 (3) Å^2 Mg1: $x=\frac{1}{8}$; $y=\frac{1}{8}$; z=0.0442 (6); occ.=1; $U_{iso}\times100$=1.3 (3) Å^2 Mg2: $x=\frac{1}{8}$; y=0.4726 (2); $z=\frac{1}{8}$; occ.=1; $U_{iso}\times100$=2.5 (4) Å^2

We used the MedeA empty space finder (ESF) [21] to analyze the empty spaces of the $CuLi_xMg_{2-x}$ supercell. The ESF algorithm divides the supercell into so-called Voronoi cells around each atom [24]. (A Voronoi cell is defined to be the volume enclosing all points that are closer to the center atom than to all other atoms). The ESF module positions non-overlapping spheres at the vertices of the resulting polyhedral grid and maximizes their radii. In doing so the physical size of different atomic species is taken into account through a set of covalent radii.

4. Results and discussion

4.1. Analysis of the diffraction data

The results from the refined data from NPDF at 60, 150 and 300 K can be found in Table 1 and indicate very good agreement between the experimental and model powder patterns. Phase fractions were varied for each pattern; the difference between the results is less than the refinement error, indicating phase stability over the investigated range of temperatures. The same statement is valid for the Li occupation and atomic parameters for both the Cu_xLiMg_{2-x} and $CuMg_2$ phases. Figs. 1–3 show the diffraction patterns at 60, 150 and 300 K and the Rietveld fits.

Results from PDF fittings at 60, 150 and 300 K can be found in Table 2 and Figs. 1–3. They indicate good agreement between the experimental and fitted curves. The error associated with each parameter obtained by PDF fitting is always higher than obtained with Rietveld, still, for 300 K where this difference is more valuable, the associated errors are $\Delta a/a$=0.45% and $\Delta c/c$=0.55% (Fig. 4).

In Fig. 4 it can be observed the result of the calculation of the lattice parameters after obtaining the slop of the interplanar distance d(Å) of the peak corresponding to the reflection (101) for Cu_xLiMg_{2-x} as a function of temperature using different values for

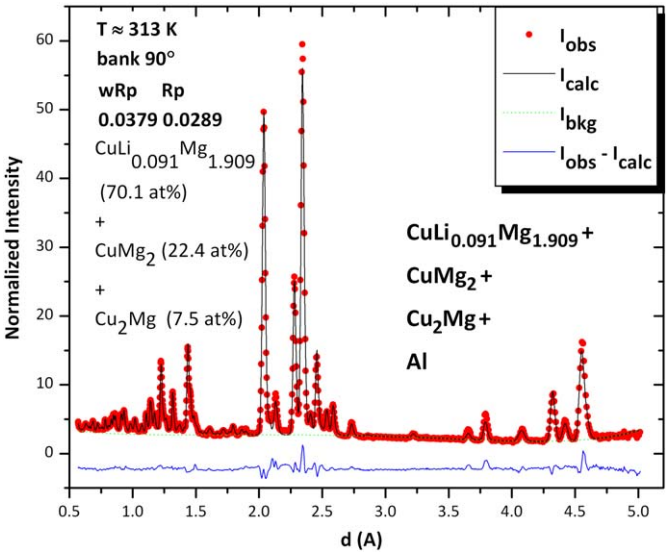

Fig. 6. HIPPO diffraction pattern at 313 K for bank 90° (the results at the graph are only due to the 90° bank).

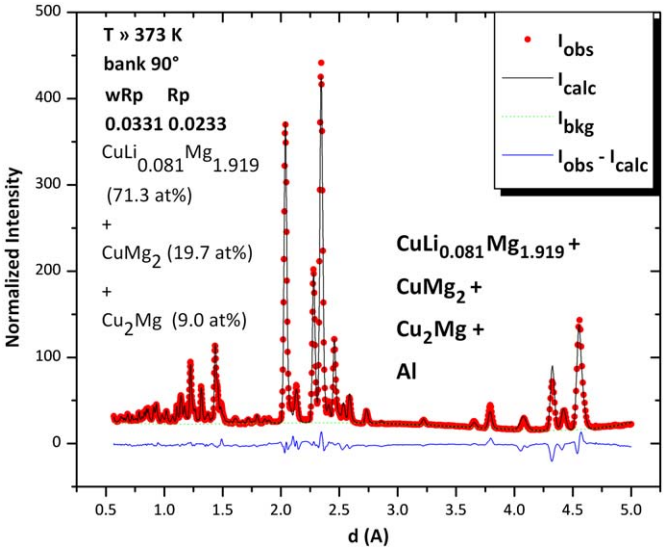

Fig. 7. HIPPO diffraction pattern at 373 K for bank 90° (the results at the graph are only due to the 90° bank).

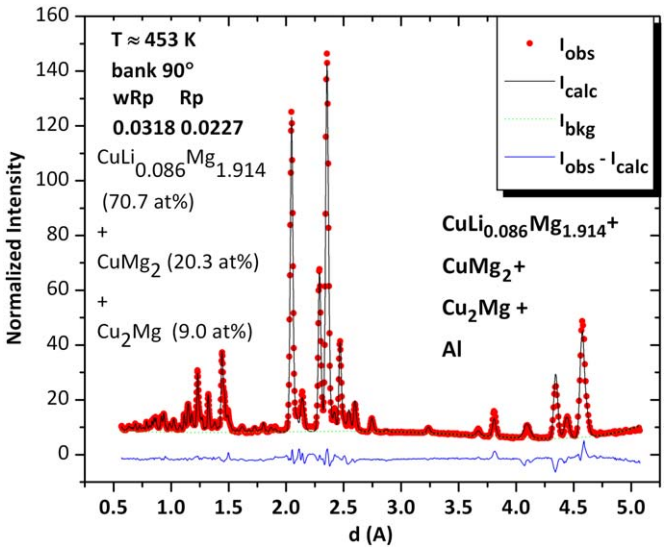

Fig. 8. HIPPO diffraction pattern at 453 K for bank 90° (the results at the graph are only due to the 90° bank).

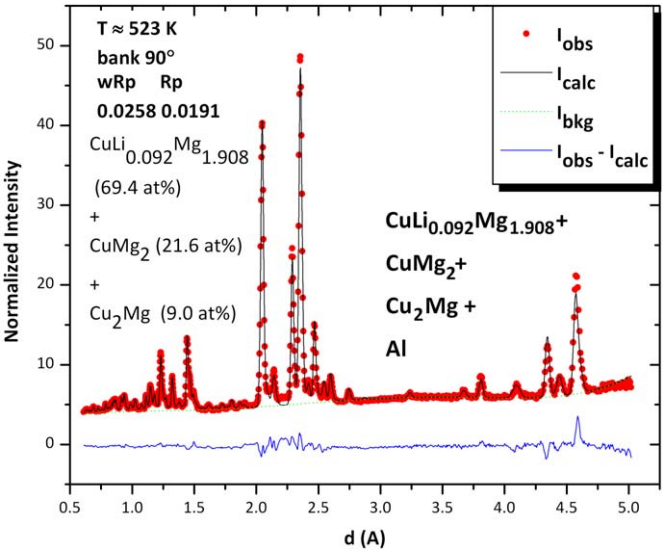

Fig. 9. HIPPO diffraction pattern at 523 K for bank 90° (the results at the graph are only due to the 90° bank).

a and c at T=0 K. Although this peak, as the other more intense non-overlapping ones, depends on both a and c lattice parameters and thus the extrapolation for a and c temperature dependence is not straight forward, we wanted to ensure that the calculations of the parameters of Cu_xLiMg_{2-x} were not interfering too much with those of $CuMg_2$ since these two phases have many overlapping peaks.

The lattice parameters of the phase Cu_xLiMg_{2-x} and the isotropic thermal parameters seem to depend linearly on temperature (Figs. 4 and 5) between 60 and 300 K.

A harmonic crystal does not undergo thermal expansion since its equilibrium size does not depend on temperature. The thermal expansion of solids is a consequence of the anharmonicity of the lattice vibrations. The earliest approach to lattice vibrations was Einstein's [25]. He proposed that all the N atoms of the crystal vibrate with $3N$ equal frequencies as harmonic oscillators. Beyond Einstein's approach, the Debye–Grüneisen approximation [26] is a good starting point for describing the contribution of lattice vibrations to the thermal expansion of solid crystals [27]. The theory is only directly applicable to crystals containing a single kind of atom; however, it has been used with success with simple compounds and with elements which do not have cubic symmetry [28]. Krishnan et al. [29] proposed an extension of Grüneisen's law for an anisotropic crystal that would depend on two different thermal expansion coefficients (with respect to $a=b$ and to c). Thus, we are expecting to find the expression of Grüneisen's law for $a=b$ and for c, independently (Fig. 4).

For metals, on the other hand, the excitation of electrons is as important as that of phonons; when included, it gives different behavior for the thermal expansion coefficient at low temperature.

We have obtained for Cu_xLiMg_{2-x} the expansion coefficient with respect to a, $\alpha_a=(1/a_{340\,K})da/dT$ (at constant pressure), approx. equal to $2.4\times10^{-5}\,K^{-1}$. The expansion coefficient with respect to c, $\alpha_c=(1/c_{340\,K})dc/dT$ (at constant pressure), is approx. equal to $0.8\times10^{-5}\,K^{-1}$. The expansion coefficient of Cu is $1.7\times10^{-5}\,K^{-1}$ and of Mg is $0.8\times10^{-5}\,K^{-1}$ at 273 K [30]. We have chosen 340 K to calculate the thermal expansion coefficient because, at this temperature, we are already in the high temperature range of our measurements.

The Debye–Waller factors, B_{iso}, that can be obtained from U_{iso} (Fig. 5), by making $B_{iso}=8\pi^2U_{iso}$ were also found to vary linearly between 60 and 300 K; additionally, all atoms seem to behave in a similar way with increasing temperature since the slope of the straight lines in Fig. 5 is very similar.

The results from the refined data from HIPPO at approximately, 313, 373, 453 and 523 K can be found in Table 3 and show good agreement between experimental and model powder patterns. On HIPPO the aluminum sample holder diffracts strongly, and the weight fraction of Cu_2Mg becomes relatively low (4–5 wt%). Refinement results for this phase were not included in Table 3 because the isotropic temperature factors became unstable and we were forced to constrain them. Still, the results seem to be very consistent *vide*, for example, Li occupancy and the atomic parameters for both the Cu_xLiMg_{2-x} and $CuMg_2$ phases. Figs. 6–9 show the diffraction patterns at 313, 373, 453 and 523 K together with the Rietveld fits.

Fig. 4 shows the difference between the XRD data and the neutron diffraction data obtained on HIPPO. Notice that the relative difference between results obtained with X-ray and obtained with neutrons never exceeds 0.4% in the case of a and 0.5% in the case of c. Additionally, the slope of the fitting line between 300 and 523 K seems to be similar in both cases. Small differences between neutron diffraction and X-ray diffraction are expected since these two techniques "see" different constituents of the atom.

The NPDF 300 K results are very similar to the 313 K HIPPO results, which is one more indicator of the results' coherence.

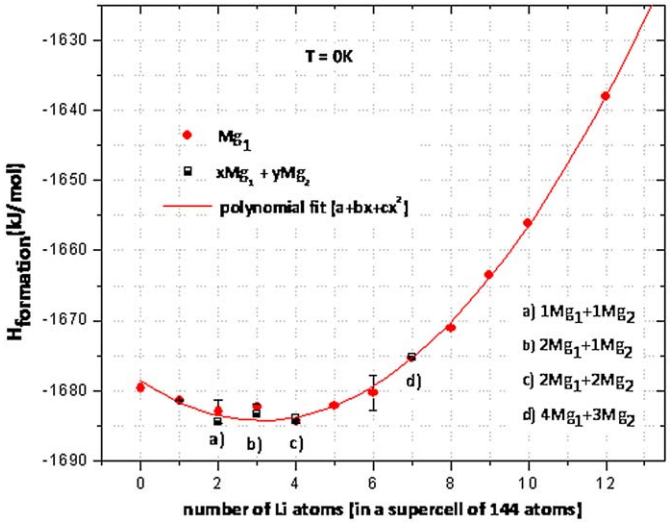

Fig. 10. First principles (*ab initio*) calculated enthalpies of formation for a mole with 144 atoms of the phase $CuLi_xMg_{2-x}$ in which 48 atoms are of Cu, $96-n$ are of Mg and n of Li ($x=n/48$). It can be observed that the most stable composition corresponds to n between 3 and 4 ($x\in$ [0.0625,0.0833]).

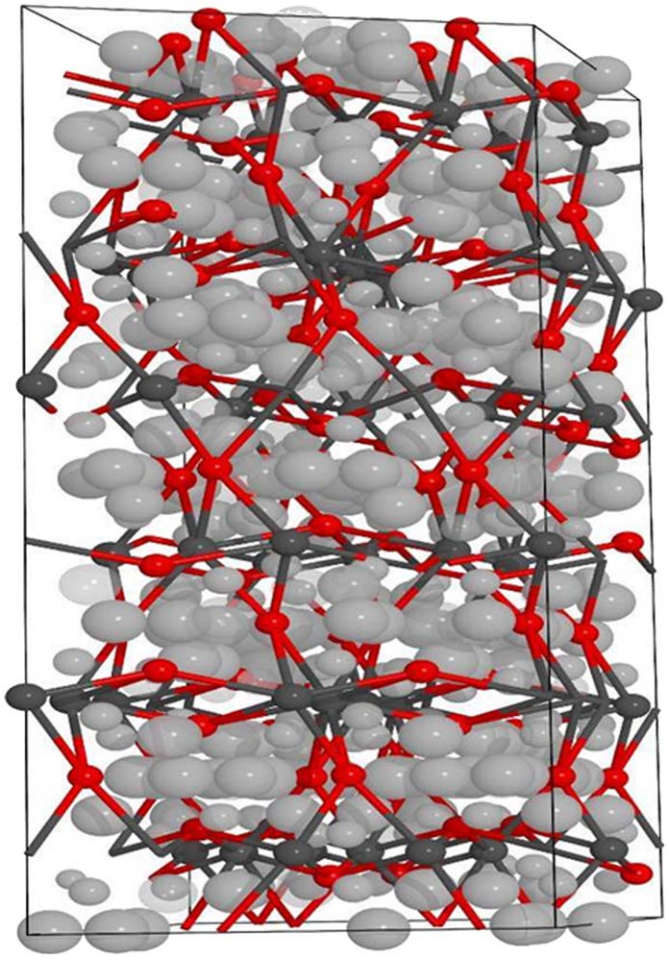

Fig. 11. Supercell of the phase $CuLi_xMg_{2-x}$ ($x=0$) with calculated empty spaces (in light grey: empty spaces, in dark grey: Cu atoms, in red: Mg atoms). (For interpretation of the references to the color in this figure legend, the reader is referred to the web version of this article.)

4.2. Analysis of the first-principles data

We studied the enthalpy of formation of the alloy $CuLi_xMg_{2-x}$ as a function of the number of Li atoms in a supercell with 144 atoms in which 48 atoms are of Cu, 96-n are of Mg and n of Li ($x=n/48$). The most stable composition (that has the lowest enthalpy of formation) corresponds to n between 3 and 4 ($x\in[0.0625,0.0833]$) (Fig. 10).

One of the purposes of this work was to determine which structure was more stable: $CuLi_{0.34}Mg_2$ (where Li occupies some of the Wyckoff 12k position of a $P6_222$ hexagonal structure) or $CuLi_xMg_{2-x}$ (with $x\cong 0.1$, in which Li occupies some of the Mg Wyckoff 6f position of a $P6_222$ hexagonal structure). For that, we have used the minimized structure of a supercell (Fig. 11) with $n=0$ ($x=0$; $CuMg_2$ with $P6_222$ hexagonal structure) and with $n=4$ ($x=0.0833$; $CuLi_{0.0833}Mg_{1.9167}$ with $P6_222$ hexagonal structure) and calculated the empty space using the ESF MedeA module (Fig. 11). Results show that in the first case the radii of the empty spaces found are $0.410\,\text{Å}\le r\le 0.650\,\text{Å}$ and in the second case $0.397\,\text{Å}\le r\le 0.666\,\text{Å}$. As the covalent radius of Li is 0.68 Å [31], we do not expect to have Li occupy interstitial sites, even if some atoms of Li substitute the Mg atoms. Still, we have tried to refine the NPDF data at 60 and 150 K for several possibilities that always contained Li atoms in interstitial sites (just in interstitial and both substituting Mg and in an interstitial site) and we have always obtained negative occupancies for these atoms.

Upon using first-principles calculations, it was not possible to determine which Mg sites are occupied with Li (Fig. 10).

In a 2007 article, Zhou et al. [32] calculated the enthalpy of formation of a mole of $CuMg_2$: $\Delta H=-13.20$ KJ/mol within the *Fddd* space group. In the present work we have obtained for $CuMg_2$ with hexagonal structure belonging to the $P6_222$ space group $\Delta H=-11.66$ KJ/mol, which is consistent with the results of Zhou et al. [32] since the orthorhombic *Fddd* structure is the stable structure for pure $CuMg_2$. What we expected is that the substitution of Mg by Li would make the *Fddd* structure of the solid solution of $CuMg_2$ less stable until $CuLi_xMg_{2-x}$ ($x=0.08$) in the hexagonal $P6_222$ structure became more stable (note that the difference between the enthalpies of formation is small, of 1.5 KJ/mol of atoms).

In the same article [32] the enthalpy of formation of $CuMg_2$ at 298 K was also determined using the CALPHAD method [33]: $\Delta H=-9.6$ KJ/mol (CALPHAD uses experimental results and theoretical models for the structure of the phases and for its Gibbs energies). The experimental value from [34] is $\Delta H=-9.55$ KJ/mol. As the enthalpy of formation of $CuMg_2$ will vary from -13.20 KJ/mol ($T=0$ K) to -9.6 KJ/mol ($T=298$ K), it still seems possible that at room temperature $CuLi_xMg_{2-x}$ ($x=0.08$) in the hexagonal $P6_222$ structure will be more stable than the orthorhombic solid solution of $CuMg_2$ for the same composition of Li. In Fig. 12, the XRD calculated pattern of $CuLi_{0.08}Mg_{1.92}$ is compared with an experimental one for a sample containing both $CuLi_{0.08}Mg_{1.92}$ and Cu_2Mg.

5. Summary

Prepared samples were invariably contaminated with Cu_2Mg, $CuMg_2$, or both. Nonetheless, the final product contained approximately 81.0 wt% (75.6 at%) of Cu_xLiMg_{2-x}, the phase we wanted to study. Thermodynamics is probably responsible for this limitation on sample composition. Indeed, preliminary tests indicate that the final amount of $CuLi_xMg_{2-x}$ material recovered depends (at the very least) on the reaction temperature and (to a lesser extent) on reaction time. We have taken advantage of this fact to extract refined parameters of $CuMg_2$ between 60 and 523 K, and of Cu_2Mg between 60 and 300 K as well as of $CuLi_xMg_{2-x}$ between 60 and 523 K.

Both neutron diffraction and first-principles calculations indicate that the composition of the ternary compound should be $CuLi_xMg_{2-x}$ ($x=0.08$).

Neither with first-principles calculations, nor with neutron diffraction, was it possible to distinguish between structures where Li substituted Mg at each of its sites individually or at both

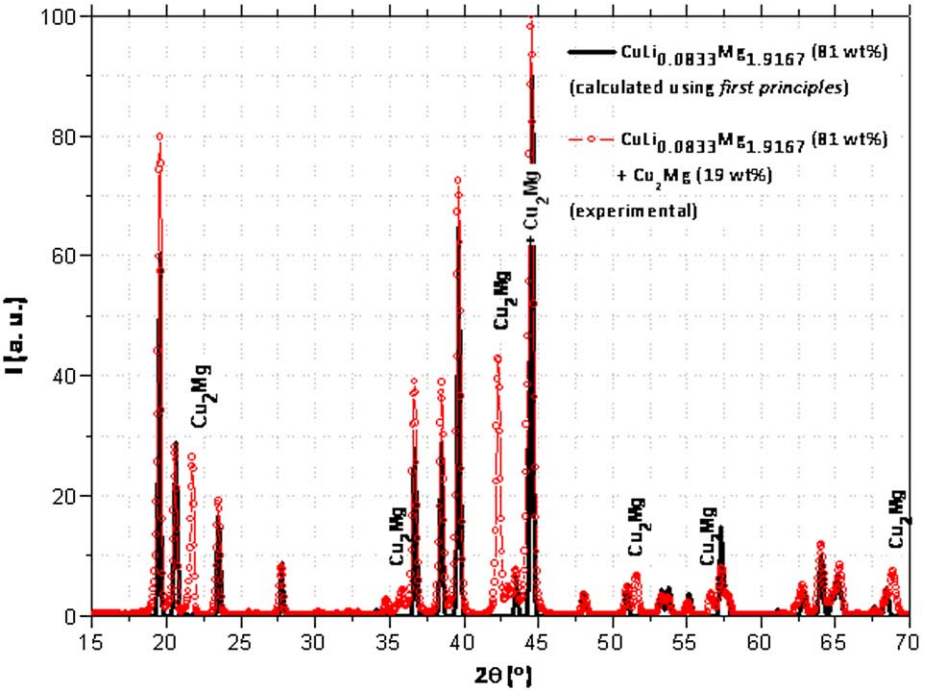

Fig. 12. Comparison between the diffraction pattern obtained using first principles and the LAZY PULVERIX code implanted in MedeA and XRD obtained at room temperature with a sample powder containing 81.0 wt% (75.6 at%) of $CuLi_xMg_{2-x}$ and 19.0 wt% (24.4 at%) of Cu_2Mg. The calculated pattern was obtained for a $B_{iso}=1.00\,\text{Å}^2$ for all the atoms.

sites. The refinement of the diffraction data revealed that the reliability factors did not change much for the three different structures, and nothing unusual happened with the other parameters (such as, for example, the Li occupancy). The calculated enthalpy of formation curve also shows differences for different occupancies of Li for the same number of Li atoms that are within the error bar. Thus we cannot draw any conclusions regarding the substituted Mg sites based on Rietveld refinement and first-principles calculations. The neutron data agrees best with the results of first-principles calculations when Li occupies Mg1 sites (1/2, 0, z). In this case, the Li occupancy corresponds to x=0.08 (in $CuLi_xMg_{2-x}$) when this value is calculated by means of Rietveld refinement and using first-principles methods. This agreement does not happen for the other possibilities. With PDF fittings we were allowed to go further. PDF does not see the average but the local structure and with PDF all results but those in which Li would substitute Mg1 sites, gave negative occupancies for Li. For Li substituting Mg1 we have obtained an average composition for $CuLi_xMg_{2-x}$ (x=0.07) which is in agreement with the other obtained results.

By calculating empty space in our structures, we found that it was unlikely that Li can occupy interstitial sites, but we note that it is possible for H to occupy these empty spaces.

Acknowledgments

M.H. Braga would like to acknowledge Portuguese Science Foundation, FCT, for the sabbatical grant (SFRH/BSAB/791/2008). This work has benefited from the use of NPDF and HIPPO at the Lujan Center at Los Alamos Neutron Science Center, funded by DOE Office of Basic Energy Sciences. Los Alamos National Laboratory is operated by Los Alamos National Security LLC under DOE Contract DE-AC52-06NA25396. The upgrade of NPDF has been funded by NSF through grant DMR 00-76488.

Appendix A. Supplementary material

Supplementary data associated with this article can be found in the online version at doi:10.1016/j.jssc.2009.09.010.

References

[1] M.H. Braga, J. Ferreira, L. Malheiros, J. Alloys Compds. 436 (2007) 278–284.
[2] M.H. Braga, L.F. Malheiros, International patent, WO2007046017.
[3] M.H. Braga, L.F. Malheiros, National patent, PT103368.
[4] M.H. Braga, A. Acatrinei, M. Hartl, S. Vogel, Th. Proffen, L. Daemen, ICNS, Knoxville, 2009.
[5] J.J. Reilly, R.H. Wiswall, Inorg. Chem. 6 (12) (1967) 2220–2223.
[6] L. Schlapbach, A. Zuttel, Nature 414 (2001) 353–358.
[7] J. Senegas, A. Mikou, M. Pezat, B. Darriet, J. Solid State Chem. 52 (1984) 1–11.
[8] V. Hlukhyy, U.Ch. Rodewald, R. Pöttgen, Z. Anorg. Allg. Chem. 631 (2005) 2997–3001.
[9] M.H. Braga, J. Ferreira, L.F. Malheiros, M. Hamaläinen, Z. Kristallogr. 26 (Suppl.) (2007) 299–304.
[10] Match, 〈http://www.crystalimpact.com/〉, 2009.
[11] P.M. de Wolff, J.W. Visser, Absolute Intensities, Report 641.109, Technisch Physische Dienst, Delft, The Netherlands. Reprinted Powder Diffract 3 (1988) 202–204.
[12] A.C. Larson, R.B. von Dreele, GSAS Generalized Structure Analysis System, LANSCE, Los Alamos, 2004.
[13] T. Egami, S.J.L. Billinge, Underneath the Bragg-Peaks: Structural Analysis of Complex Materials, Elsevier Science B.V., Amsterdam, 2003.
[14] C.L. Farrow, P. Juhas, J.W. Liu, D. Bryndin, E.S. Bozin, J. Bloch, Th. Proffen, S.J.L. Billinge, J. Phys. Condens. Matter 19 (2007) 335219.
[15] P. Hohenberg, W. Kohn, Phys. Rev. 136 (1964) B864.
[16] W. Kohn, L.J. Sham, Phys. Rev. 140A (1965) 1133.
[17] J.P. Perdew, Y. Wang, Phys. Rev. B 45 (1992) 13244.
[18] C. Colinet, Intermetallics 11 (2003) 1095–1102.
[19] P.E. Blochl, Phys. Rev. B 50 (1994) 17953.
[20] G. Kresse, J. Furthmüller, Phys. Rev. B 54 (1996) 11169;
G. Kresse, J. Furthmüller, Comp. Mater. Sci. 6 (1996) 1;
G. Kresse, D. Joubert, Phys. Rev. B 59 (1999) 1758.
[21] MedeA, Materials Design, Inc., 〈http://www.MaterialsDesign.com〉, 2009.
[22] J.P. Perdew, K. Burke, M. Ernzerhof, Phys. Rev. Lett. 77 (1996) 3865;
J.P. Perdew, K. Burke, M. Ernzerhof, Phys. Rev. Lett. 78 (E) (1997) 1396.
[24] G. Voronoi, J. für die Reine und Angew. Math. 133 (1907) 97–178.
[23] K. Yvon, W. Jeitschko, E. Parthe, J. Appl. Cryst. 10 (1977) 73–74.
[25] A. Einstein, Ann. Phys. (Leipzig) 22 (1907) 180–800;
A. Einstein, Ann. Phys. (Leipzig) 34 (1911) 170 590.
[26] P. Debye, Ann. Phys. (Leipzig) 33 (1910) 442–489.
[27] T.H.K. Barron, M.L. Klein (1962) reedited in Phys. Rev. 127 (1997) 77.
[28] F. Sayetat, P. Fertey, M. Kessler, J. Appl. Cryst. 31 (1998) 121–127.
[29] R. Krishnan, R. Srinivasan, S. Devanarayan, Thermal Expansion of Crystals, Pergamon Press, London, 1979.
[30] Web Elements periodic table, 〈http://www.webelements.com/periodicity/coeff_thermal_expansion/〉, 2009.
[31] Cambridge Crystallographic Data Centre, 〈http://www.ccdc.cam.ac.uk/products/csd/radii/〉, 2008.
[32] S. Zhou, Y. Wang, F.G. Shi, F. Sommer, L.-Q. Chen, Z.-K. Liu, R.E. Napolitano, JPEDAV 28 (2007) 158–166.
[33] H.L. Lukas, S.G. Fries, B. Sundman, Computational Thermodynamics The Calphad Method, Cambridge, 2007.
[34] R.C. King, O.J. Kleppa, Acta Metall. 12 (1964) 87–97.